LBNL-51928

On Leakage and Seepage from Geologic Carbon Sequestration Sites:

Unsaturated Zone Attenuation

Curtis M. Oldenburg* and André J. A. Unger

Earth Sciences Division 90-1116
Lawrence Berkeley National Laboratory
University of California
Berkeley CA 94720, USA

cmoldenburg@lbl.gov

(510) 486-7419

Fax: (510) 486-5686

*Corresponding author

22 April 2003

Abstract

Geologic carbon sequestration is the direct injection of carbon dioxide (CO_2) into deep geologic formations for permanent disposal. Although numerous trapping mechanisms exist in the subsurface, it is possible that CO_2 will leak from the primary sequestration target and seep out of the ground. The unsaturated zone has the potential to attenuate leaking CO_2 and decrease seepage and near-surface CO_2 concentrations. Attenuation processes include permeability trapping, ponding as dense CO_2 spreads out on the water table, solubility trapping by infiltrating or residual water, and dilution through mixing with ambient soil gas. Numerical simulations of CO_2 flowing upward through a thick model unsaturated zone were carried out to investigate the sensitivity of various unsaturated zone properties on CO_2 seepage flux and near-surface CO_2 gas concentrations. These two quantities are considered drivers for health and environmental risk due to exposure to CO_2. For the conceptual model considered, seepage flux and near-surface CO_2 gas concentrations are most strongly controlled by the leakage rate at the water table, followed by the source zone radius. Permeability and permeability anisotropy, as well as porosity and infiltration rate are also important, although to a lesser degree. Barometric pumping causes local maxima in seepage flux and near-surface CO_2 concentrations, but has negligible effect in a time-averaged sense. When the leakage source is turned off, the CO_2 plume attentuates through dissolution into infiltrating water. For the case of a constant leakage rate, the unsaturated zone can attenuate low leakage fluxes but should not be expected to attenuate large CO_2 leakage fluxes.

Introduction

Geologic carbon sequestration is one strategy for reducing the rate of increase of global atmospheric carbon dioxide (CO_2) concentrations (IEA, 1997; Reichle, 1999). As used here, the term geologic carbon sequestration refers to the direct injection of liquid or supercritical CO_2 deep into subsurface geologic formations. The target formations will typically be either depleted oil and gas reservoirs, or brine-filled permeable formations. The idea is to trap injected CO_2 by one or more of the following mechanisms (e.g., Bachu et al., 1994): (1) permeability trapping, for example when buoyant supercritical CO_2 rises until trapped by a confining layer or cap rock; (2) solubility trapping, for example when CO_2 dissolves into the aqueous phase in the pore space, or (3) mineralogic trapping, such as occurs when CO_2 reacts to form stable carbonate minerals. When CO_2 is trapped in the subsurface by any of these mechanisms, it is effectively sequestered away from the atmosphere where it would otherwise act as a greenhouse gas.

Although the purpose of geologic carbon sequestration is to trap CO_2 in the subsurface, there is the risk that injected CO_2 will migrate away from the primary target formation (Holloway, 1997). Migration away from the primary target formation is referred to here as *leakage*. Carbon dioxide that leaks from the primary sequestration target and moves up through subsurface formations will likely undergo secondary trapping in up-section structural traps and by dissolution processes, resulting in very long transport times (Lindeberg, 1997). This is in contrast to leakage that may occur through a well or other fast-flow path, in which case subsurface gas transport can be very fast (e.g., Allison, 2001). If CO_2 reaches the shallow subsurface or migrates out of the ground into the

ambient air, health and environmental risks can arise. In analogy to existing processes whereby water, oil, and gas migrate across the subsurface–ground-surface interface, we refer to the migration of CO_2 out of the ground as *seepage*. Seepage of CO_2 can lead to locally high CO_2 concentrations, especially in topographic depressions because CO_2 is a dense gas relative to air. Ambient CO_2 concentrations in the atmosphere are approximately 350 ppmv, while CO_2 concentrations of 1% or more cause measurable adverse physiological effects, and concentrations above 10% can be deadly (NIOSH, 1976).

The objective of this work is to examine the potential of the unsaturated zone to attenuate CO_2 leaking from a geologic sequestration site. This is in contrast to prior studies that have focused on ambient soil processes (e.g., Amundsen and Davidson, 1990; Kawbe et al., 2002). Attenuation processes include CO_2 gas ponding on the water table due to its high density, permeability trapping, solubility trapping, and simple dilution by mixing with ambient soil gas. We are not considering mineralogic trapping which generally occurs on a time scale much longer than gas transport in the vadose zone. Direct interaction with the atmosphere is considered in terms of barometric pumping, although the effects of winds on shallow soils are beyond the scope of this study. With an aim toward contributing to analyses of potential health and environmental risk due to CO_2 seepage, we present simulation results in terms of seepage flux and near-surface CO_2 concentrations, both of which are drivers of exposure risk for humans and other living things in the biosphere. Rather than defining a detailed or site-specific unsaturated zone, we have adopted the approach of a sensitivity analysis. In this approach, the effects of

various properties of a model system, for example leakage rate, permeability, radius of leakage zone, porosity, and infiltration rate can be simulated. This approach determines the trends in seepage flux and near-surface CO_2 concentrations for natural systems with various combinations of properties. The sensitivity analysis is based on a conceptual model in which CO_2 is discharged at the water table at a constant rate, for example through a high-permeability zone with direct connection to the target sequestration formation, and migrates upward through a thick unsaturated zone. Finally, we also consider a single case in which the leak is turned off and the CO_2 plume is controlled by density and infiltration effects.

Methods

The approach we use to investigate leakage and seepage of CO_2 in the subsurface is numerical simulation. Simulations presented in this work were performed using TOUGH2 (Pruess et al., 1999) with a special module called EOS7CA applicable to flow and transport of CO_2 and air in subsurface systems. TOUGH2/EOS7CA models the subsurface flow and transport of aqueous and gas phases containing five components (H_2O, brine, CO_2, gas tracer, and air) under isothermal or nonisothermal conditions. TOUGH2/EOS7CA uses real gas mixture properties calculated using the Peng-Robinson equation of state model. Air is approximated in EOS7CA as a mixture of 79% nitrogen and 21% oxygen by volume. Solubility of CO_2 in the aqueous phase is modeled by Henry's Law, with Henry's coefficients calculated from Cramer (1982). Viscosity is estimated using the method of Chung et al. (1988) as described by Poling et al. (2001).

Gas Properties

The physical properties of CO_2 relative to air and liquid water have a significant impact on the ability of the subsurface to attenuate leaking CO_2. Carbon dioxide is a colorless and odorless gas with critical pressure (P_c) equal to 73.8 bars and critical temperature (T_c) equal to 31°C. We present in Figure 1 the phase diagram for CO_2 showing the gaseous, liquid, solid, and supercritical regions along with an approximate curve representing a *P-T* path in the subsurface assuming hydrostatic pressure and 25°C km^{-1} geothermal gradient. As shown in Figure 1, the geothermal gradient ensures that CO_2 will be supercritical in the subsurface at depths greater than approximately 800 m, and gaseous at shallower depths.

The density of CO_2 increases drastically as it changes from subcritical to supercritical conditions, however, the geothermal gradient ensures a sufficiently high temperature that CO_2 is buoyant relative to water in the saturated zone. Shown in Figure 2 is the density of CO_2 as a function of pressure at three different temperatures, where the symbols show results from TOUGH2/EOS7CA and the lines are from the NIST14 database (NIST, 1992). Because the focus in this paper is the unsaturated zone, we present in Figure 3 the density of CO_2 and air mixtures at 1 bar. As shown, pure CO_2 at 1 bar and 20 ˚C has a density of approximately 1.8 kg m^{-3} while pure air has a density of 1.2 kg m^{-3}. The effects of water vapor in the air will further decrease ambient soil gas density. Thus, the high density of CO_2 relative to soil gas creates the potential for CO_2 to pond on the water table, and resist moving upwards to the ground surface. In summary, Figures 2 and 3 show that while CO_2 will tend to rise upward in the saturated zone, it may tend to

accumulate in the unsaturated zone and in topographic depressions due to its high density.

Other transport properties of CO_2 are also relevant to leakage attenuation. In particular, the solubility of CO_2 in water is relatively high, approximately 50 times that of air at 1 bar, 20 ˚C. The large solubility of CO_2 has the potential to attenuate CO_2 by solubility trapping in water in the unsaturated zone. At 1 bar and 20 ˚C, CO_2 is slightly less viscous and therefore more mobile than air ($\mu_{CO2} = 1.5 \times 10^{-5}$ Pa s, $\mu_{air} = 1.8 \times 10^{-5}$ Pa s) (NIST, 1992). At ambient atmospheric conditions of 1 bar and 10 °C, the free gas molecular diffusivity of CO_2 in air is typical of other gases and is of order 10^{-5} m^2 s^{-1} (Vargaftik, 1975). Simulation results presented here use the Fickian advective-diffusive model for gas transport, a good approximation for high-permeability systems (Webb, 1998; Oldenburg et al., 2003).

Conceptual Model

The conceptual model for attenuation of leakage by the unsaturated zone is based on a prototypical geological sequestration site containing a mass of 4×10^9 kg of CO_2. The hydrogeological properties of the system for the base case are listed on Table 1. These properties are typical of poorly sorted and unconsolidated sediments such as can be found in California's Central Valley. Figure 4 depicts the conceptual model and grid used to simulate the transport of CO_2 through the unsaturated zone. The model is cylindrical with the Cartesian axis located in the z-direction. The model unsaturated zone is 30 m thick, with a saturated zone 5 m in thickness. The mesh used for simulations contains

20×120 nodes with a minimum and maximum radial size of 5 m and 30 m, respectively. The vertical discretization is uniformly 1.75 m. Temperature is assumed to be constant at 15°C throughout the domain.

For the base case, CO_2 is introduced into the model system over a radial distance of 100 m, which corresponds to an area of 3×10^4 m^2 over which leakage of CO_2 from the reservoir arrives at the water table. This area is small relative to the expected geologic sequestration site footprint and represents a focused leak as might occur along intersecting subnormal faults. The leakage rates used were 4×10^4 kg yr^{-1}, 4×10^5 kg yr^{-1}, and 4×10^6 kg yr^{-1} representing leakage rates of 0.001%, 0.01%, and 0.1% per year of the initial mass of a 4×10^9 kg CO_2 sequestration reservoir. For reference, an overall leakage rate of 0.01% per year or less would still meet atmospheric stabilization targets, and 0.1% per year is effective for some energy and population scenarios (see Hepple and Benson, 2002).

The bottom boundary is held at hydrostatic pressure while the top boundary is used to enforce an atmospheric pressure equal to 1 bar. In addition, the gas-phase CO_2 concentration at the top of the system is held at 350 ppmv. Recharge water enters the top of the domain uniformly in equilibrium with the 350 ppmv atmospheric CO_2 concentration as controlled by Henry's law. The right-hand side boundary is constant pressure (hydrostatic below the water table, and gas-static in the unsaturated zone). The left-hand side boundary is no-flow appropriate for symmetry about the z-axis.

Sensitivity Analysis Method

In order to focus the analysis on the ability of the unsaturated zone to attenuate leakage of CO_2, we have adopted a worst-case scenario where we assume that CO_2 from the leaky sequestration target reservoir discharges directly at the water table. Such a release could occur as the result of a high-permeability conduit that allows fast flow through the saturated zone circumventing likely attenuating influences in the saturated zone such as secondary solubility and permeability trapping. The objective of this analysis is to determine the influence of hydrogeological properties of the unsaturated zone and leakage characteristics on the maximum seepage flux of CO_2 as well as the maximum near-surface mole fraction of CO_2 relative to the base scenario. Specifically, we varied six parameters including the source zone leakage rate, permeability, permeability anisotropy, source zone radius, porosity, and infiltration rate. For this analysis, the unsaturated zone is relatively thick at 30 m. Suffice it to say that attenuation by the unsaturated zone will be generally smaller for cases where the water table is nearer the surface. Permeabilities in the range 10^{-12}–10^{-9} m^2 were chosen to represent a permeable unsaturated zone, and extrapolation to lower or higher permeabilities can be made from the sensitivity study presented below. Hydrogeological properties for the base case are presented in Table 1. The potential exposure risk to CO_2 at the ground surface will be put into perspective by comparison to both a typical ecological CO_2 efflux taken as 4.4×10^{-7} kg s^{-1} m^{-2} or 10 μmol s^{-1} m^{-2} (Baldocchi and Wilson, 2001) as well as the mole fraction of CO_2 in the gas phase in soil at which tree mortality has been observed, taken as 0.3 (e.g., Farrar et al., 1995; 1999).

Results

Leakage Rate

Results are shown in Figure 5 as vertical cross-sections showing mass fraction of CO_2 in the gas phase, water saturation, and gas phase pore velocity vectors for leakage rates of (a) 4×10^4 kg yr^{-1}, (b) 4×10^5 kg yr^{-1}, and (c) 4×10^6 kg yr^{-1} after relatively steady seepage rates are obtained after 100 years. These figures show that although the CO_2 mass fraction is nearly unity above the source, and therefore forms a dense gas phase relative to ambient soil gas, there is very little lateral spreading of CO_2 on the water table. In fact, the CO_2 plume spreads a maximum of 120 m beyond the radius of the source zone for the highest leakage rate. Instead, the CO_2 plume reaches the ground surface for all injection rates. However, it should be kept in mind that the radial geometry involved ensures that there is a significant mass of CO_2 contained within the region where spreading has occurred between 100 and 120 m from the axis of the system.

The temporal evolution of the total seepage and maximum near-surface CO_2 concentrations are presented in Figure 6 for three different leakage rates. The maximum CO_2 concentration at the top always occurs at the center (left-hand side) of the model system. With time beginning when the leakage reaches the water table, the results show that the unsaturated zone retards seepage but the retardation time depends strongly on the leakage rate. For the largest leakage rate, the unsaturated zone retards CO_2 seepage by only several days, while for the lowest leakage rate, it retards CO_2 by nearly a year. As shown, the total seepage and maximum CO_2 concentrations at the surface are nearly steady after approximately 50 years for the three leakage rates tested.

Permeability and Permeability Anisotropy

Additional example simulation results are shown in Figure 7 for comparison to the base case shown in Figure 5. Figures 7a and 7b show vertical cross-sections of the mass fraction of CO_2 in the gas phase, water saturation, and gas-phase pore velocity vectors for a leakage rate of 4×10^5 kg yr^{-1} for a permeability (k) of 1×10^{-9} m^2 and an anisotropy (k_r:k_z) of 1000:1, respectively. By comparing Figure 5b with Figure 7a, we observe that as both the horizontal and vertical permeabilities are increased from 1×10^{-12} m^2 to 1×10^{-9} m^2, horizontal spreading of the plume increases dramatically while vertical transport is reduced. Comparison of Figures 5b and 7b reveals that as the anisotropy is increased from 1:1 to 1000:1, the same trend of increased horizontal spreading and decreased vertical transport occurs. This trend is more prominent for the anisotropy case because the vertical permeability, k_z, remains fixed at the lowest value of 1×10^{-12} m^2 forcing the CO_2 to be preferentially transported horizontally.

Source Zone Radius

The radius of the source zone over which leakage occurs strongly controls unsaturated zone leakage attenuation. Consideration of a very small source radius corresponds to the assumption that the migration pathway that CO_2 has followed to the water table is confined to a small zone, such as a borehole, while a large radius is consistent with a model in which CO_2 migration occurs through multiple fracture zones or widespread permeable formations. As part of a sensitivity analysis, we adjusted the source radius from the base-case value of 100 m to a maximum value of 1000 m and a minimum value of 10 m. All hydrogeological parameters shown on Table 1 were held constant. The leakage rate was also varied from 4×10^6 kg yr^{-1} to 4×10^5 kg yr^{-1} and 4×10^4 kg yr^{-1}.

Figures 5b, 7c and 7d show vertical cross section results for a leakage rate of 4×10^5 kg yr^{-1} with a source radius of 100 m, 10 m, and 1000 m, respectively. As the source radius is decreased by an order-of-magnitude to 10 m, the gas-phase pressure increases significantly around the source zone perturbing the water table. The width of the CO_2 plume emanating from the 10 m source zone is only slightly smaller than that of the base case (Figure 5b). This indicates that for a leakage rate of 4×10^5 kg yr^{-1}, the CO_2 plume extends out a minimum radial distance of 130 m from the origin and is not simply confined to a radius of the source zone as might be inferred from the base case. As the source radius is increased by an order-of-magnitude to 1000 m, the flux of CO_2 decreases dramatically yielding significantly lower mole fractions of CO_2 in the gas phase above the source zone.

Porosity

The porosity of the unsaturated zone has the potential to influence the horizontal and vertical transport of the CO_2 plume by changing the pore volume available to the gas phase CO_2 plume. A decrease in porosity should increase the gas velocity and plume size while an increase in porosity should decrease gas velocity and plume size. As part of a sensitivity analysis, we doubled the porosity from the base-case value of 0.2 to 0.4 and alternatively halved it to 0.1. All other hydrogeological parameters shown on Table 1 were held constant. The leakage rate was also varied from 4×10^6 kg yr^{-1} to 4×10^5 kg yr^{-1} and 4×10^4 kg yr^{-1}. Results are summarized in Figure 8 as described below.

Infiltration Rate

Water infiltrating through the unsaturated zone is in equilibrium with atmospheric concentrations of CO_2 that are orders-of-magnitude lower than the values above the source zone in the base case. Therefore, this water has the capacity to attenuate the upward migration of CO_2 through the unsaturated zone as it continually dissolves CO_2 from the gas phase. As part of a sensitivity analysis, we increased the infiltration rate from the base-case value of 0.1 m yr^{-1} to 0.5 m yr^{-1}, and decreased it to 0.02 m yr^{-1} and 0.0 m yr^{-1}. All hydrogeological parameters shown on Table 1 were held constant. The leakage rate was also varied from 4×10^6 kg yr^{-1} to 4×10^5 kg yr^{-1} and 4×10^4 kg yr^{-1}. Results of this sensitivity study are presented in Figure 8, to be discussed below.

Summary of Sensitivity Analysis

Results from a multitude of simulations are presented in Figure 8 as a comprehensive summary of the sensitivity analyses we have carried out. Figures 8a and 8b show leakage rate on the x-axis versus seepage rate and maximum near-surface CO_2 mole fraction in the gas, respectively, on the y-axis. The first conclusion to be drawn from Figure 8 is that the main parameter controlling the seepage and concentration of CO_2 at the ground surface is the leakage rate from the reservoir. For our base-case scenario, the maximum leakage rate that could be simulated without significantly perturbing the water table was 4×10^6 kg yr^{-1}, corresponding to 0.1% yr^{-1} leaking from the reservoir. As the leakage rate decreases from 4×10^6 kg yr^{-1}, the maximum seepage flux of CO_2, which always occurs at the center of the radial system, drops below that of the ecological flux. Although the maximum seepage flux of CO_2 appears to be quite small, the corresponding maximum

near-surface mole fraction of CO_2 may pose a significant health and environmental risk. This is indicated by values above the 0.3 mole fraction tree mortality level as shown in Figure 8b.

Figure 8 shows that the smallest source radius causes the greatest seepage of CO_2 for a given leakage rate. As the source zone radius increases from 10 m to 100 m and 1000 m, the seepage of CO_2 drops dramatically for all three leakage rates. Specifically, the maximum seepage flux of CO_2 is significantly larger than the typical ecological flux except at the lowest leakage rate. For comparison, the seepage for a leakage rate of 4×10^6 kg yr^{-1} approaches the maximum values measured around the Horseshoe Lake tree-kill area at Mammoth Mountain, CA (Sorey et al., 1999). Not surprisingly, the maximum near-surface mole fraction of CO_2 also exceeds the tree-mortality limit. As the source radius is increased to 1000 m, the CO_2 seepage and near-surface concentration are below the ecological flux and tree mortality limits for all three leakage rates.

After the leakage rate and leakage area, the next most sensitive parameters controlling the seepage and near-surface concentration of CO_2 are the permeability and anisotropy of the unsaturated zone. As part of a sensitivity analysis, we increased the radial and vertical permeabilities, k_r and k_z, from the base-case value of 1×10^{-12} m^2 to 1×10^{-11} m^2, 1×10^{-10} m^2, and 1×10^{-9} m^2. Similarly, we also increased the anisotropy of k_r:k_z from 1:1 in the base case to 10:1, 100:1, and 1000:1. All other hydrogeological parameters shown on Table 1 were held constant. The sensitivity of the seepage and near-surface CO_2 concentrations to an increase in the permeability and the anisotropy is also shown on Figure 8. For a

leakage rate of 4×10^{6} kg yr^{-1}, the maximum seepage flux of CO_2 is relatively insensitive to an increase in permeability but is very sensitive to an increase in anisotropy. Specifically, the maximum seepage flux of CO_2 is greater than the typical ecological flux for the full range of permeabilities used in the sensitivity analysis, whereas only an anisotropy ratio of 1:1 and 10:1 are greater than the ecological flux. As the leakage rate decreases to 4×10^{5} kg yr^{-1} and 4×10^{4} kg yr^{-1}, the seepage flux is always less than the ecological flux independent of variations in permeability and porosity. For a leakage rate of 4×10^{6} kg yr^{-1}, the maximum near-surface mole fraction of CO_2 exceeds the tree mortality value of 0.3 for all ranges of permeability and all values of anisotropy from 1:1 to 100:1. As the leakage rate decreases to 4×10^{5} kg yr^{-1}, both a permeability of 1×10^{-11} m^2 and an anisotropy of 10:1 are close to the tree mortality limit with all other values of permeability and anisotropy below this threshold.

Results for maximum seepage flux and near-surface mole fraction of CO_2 for infiltration rates of 0.1 m yr^{-1} (base case), 0.0 m yr^{-1}, 0.5 m yr^{-1} and 0.02 m yr^{-1} are also shown in Figures 8a and 8b. These results show that the CO_2 seepage and near-surface concentrations do not deviate significantly from the base case as the infiltration rate changes. Figure 8 also shows the maximum surface flux and near-surface mole fraction of CO_2 for porosities of 0.2 (base case), 0.4, and 0.1. These results also do not deviate significantly from the base case due to variability in porosity for all three leakage rates.

We have also investigated the effects of barometric pumping on the seepage and near-surface mole fraction of CO_2. We specified a time-varying top pressure boundary

condition corresponding to an actual pressure variation measured in the Central Valley of California for the year 1997 and carried out a simulation with properties of the base case. This pressure profile, shown in Figure 9, was assumed to repeat annually in our simulations. Results of the maximum seepage flux and near-surface mole fraction are shown as a function of time (log scale) in Figure 10. As shown, the time-averaged effect of barometric pumping on seepage and shallow CO_2 concentration is negligible, even though locally higher and lower fluxes and concentrations can arise from day-to-day variations in pressure. Furthermore, the small leakage rate cases show larger amplitude variation as barometric pumping occurs because the air flow driven by atmospheric pressure variation dominates over the CO_2 leakage flux for small CO_2 fluxes. The lack of importance of barometric pumping observed in these simulations arises from the cyclic nature of barometric pressure variation. Wind forcings that act more consistently in one direction are expected to influence the shallowest soil layers and will tend to enhance CO_2 seepage and dilute shallow soil gas CO_2 concentrations, but are beyond the scope of this study.

Another scenario relevant to the unsaturated zone is the case where the CO_2 leakage is eventually detected and the leak is effectively stopped, for example by means of operations to lower the pressure in the leaking CO_2 sequestration reservoir. We considered a single case of this scenario by starting from the steady-state solution (t = 100 yrs) of the 4 x 10^6 kg yr^{-1} leakage rate case and then turning off the CO_2 source. In this case, the driving force for the CO_2 plume will evolve to depend on density effects and dissolution as infiltration passes through the plume. Presented in Figure 11 are cross-

sections of the simulated results after 6 months, 1 year, 5 years, and 10 years. Note that between 6 months and 1 year, a small amount of lateral spreading occurs, and the near-surface CO_2 concentrations rapidly decrease as the plume dissolves in the infiltrating water. Large-scale effects of lateral density-driven flow are not observed because the pressurization arising from the prior injection at the water table dominates over the buoyancy effects for the entire period prior to when the plume dissipates through dissolution into infiltrating water. However, gas-phase velocities rapidly diminish after the source is turned off. For comparison, gas-phase velocity vectors are approximately 100 times smaller after 6 months, and 1000 times smaller after 10 years than the steady state initial condition shown in Figure 5c. As shown, infiltration in the unsaturated zone is very effective at attenuating CO_2 plumes that are not being continuously replenished by leakage from below for this particular conceptual model.

In Table 2 we summarize the flow rates, attenuation efficiencies, storage rates, and inventories of the unsaturated zone as a function of the three different leakage rates for the base case. The attenuation efficiency is defined as one minus the ratio of CO_2 seepage rate to the CO_2 leakage rate when the seepage rate reaches an approximate steady-state, in this case after 1000 years. As shown in Table 2, the seepage rate increases nonlinearly with the leakage rate. The reason for this is that smaller leakage rates result in more lateral spreading and CO_2 capture by downward-moving infiltration relative to larger leakage rates. The physical process limiting the lateral spreading of CO_2 is the downward advection of CO_2 dissolved in infiltrating water, and the subsequent discharge of this CO_2 through the lower hydrostatic boundary condition. For the lowest

leakage rate of 4×10^4 kg yr^{-1}, the attenuation efficiency of the unsaturated zone is 96%, while for the highest leakage rate of 4×10^6 kg yr^{-1}, the attenuation efficiency is 19%. The attenuation efficiency of the unsaturated zone decreases with increasing leakage rate because the higher pressures surrounding the source zone force more vertical flow that directly causes seepage of CO_2 above the source zone. We note also from Table 2 that the amount of CO_2 crossing the lower boundary increases as the leakage rate increases, but at a fraction of the rate of increase of the seepage. Essentially, the downward infiltrating water cannot transport all of the CO_2 being introduced to the system and increasing amounts end up seeping out of the ground. The rate at which CO_2 is being stored in the aqueous and gas phases at 1000 years is defined as the leakage plus infiltration minus the seepage and minus the bottom boundary loss. For small leakage rates, the ratio of seepage to storage is very small showing the effectiveness of the unsaturated zone in attenuating leakage migration to the surface. For higher leakage rates, the ratio of seepage to storage increases showing the ineffectiveness of the unsaturated zone in attenuating high leakage fluxes. As for the inventories, note again that the total amounts present in the aqueous and gas phases increase as some fractional power of the leakage rate.

Conclusions

This work focused on determining the potential of the unsaturated zone to attenuate CO_2 from leaking geologic carbon sequestration sites. The conceptual model involved CO_2 reaching the water table at a constant rate, for example through a potential high-permeability zone with direct connection to the target formation. We use the maximum

seepage flux of CO_2 across the ground surface as well as the maximum mole fraction of CO_2 just below the ground surface as rough indicators of exposure risk. The potential risk posed was put into perspective by comparing results to both a typical ecological flux of CO_2 taken as 4.4×10^{-7} kg m^{-2} s^{-1} as well as the mole fraction of CO_2 (0.3) in the gas phase in soil at which tree mortality has been shown to occur.

Results from the unsaturated zone conceptual model indicate that the source zone leakage rate combined with source zone radius have the greatest influence on the maximum seepage flux of CO_2 as well as the maximum mole fraction of CO_2. Once the CO_2 reaches the unsaturated zone, it forms a gas phase that is denser than that of the ambient soil gas. Pressure gradients between the source zone at the water table and the ground surface easily overcome this density contrast for all leakage rates tested, causing CO_2 to discharge at the ground surface. The pressure driving force is significantly reduced by increasing the source zone radius, but not by adjusting hydrogeological properties of the unsaturated zone such as the permeability, anisotropy, infiltration rate, and porosity.

The unsaturated zone conceptual model was used to calculate the steady-state seepage rate for a prescribed leakage rate. For the lowest leakage rate of 4×10^{4} kg yr^{-1}, the unsaturated zone attenuated 96% of the CO_2 after 100 years. For the highest leakage rate of 4×10^{6} kg yr^{-1}, the attenuation efficiency of the unsaturated zone decreased substantially to 19%. The attenuation efficiency of the unsaturated zone decreased with increasing leakage rate because the higher pressures surrounding the source zone caused more

vertical migration of the CO_2 relative to lateral migration which is more strongly affected by infiltration.

Barometric pumping has a negligible effect on the time-averaged seepage flux and near-surface CO_2 concentration because of the cyclic nature of the pressure-induced flows. For a CO_2 plume present in the unsaturated zone with no continuous replenishment, dissolution into infiltrating water causes relatively rapid attenuation.

Acknowledgments

We thank Karsten Pruess and Christine Doughty (LBNL) for constructive review comments, and Sally Benson, Marcelo Lippmann, Robert Hepple, and Preston Jordan (all LBNL) for stimulating discussions that helped focus the study. This work was supported in part by a Cooperative Research and Development Agreement (CRADA) between BP Corporation North America, as part of the CO2 Capture Project (CCP) of the Joint Industry Program (JIP), and the U.S. Department of Energy (DOE) through the National Energy Technologies Laboratory (NETL), and by the Office of Science, U.S. Department of Energy under contract DE-AC03-76SF00098.

References

Allison, M.L., Hutchinson, Kansas: A geologic detective story; *Geotimes*, *46*(10, 14–20, October 2001.

Amundsen, R.G., and E.A. Davidson, Carbon dioxide and nitrogenous gases in the soil

atmosphere, *J. of Geochem. Explor.*, *38*, 13–41, 1990.

Bachu, S., W.D. Gunter, and E.H. Perkins, Aquifer disposal of CO_2 – Hydrodynamic and mineral trapping, *Energy Convers. Mgmt.*, *35*(4), 269–279, 1994.

Baldocchi, D.D., and K.B. Wilson, Modeling CO_2 and water vapor exchange of a temperate broadleaved forest across hourly to decadal time scales, *Ecological Modelling*, *142*, 155–184, 2001.

Chung, T.-H., M. Ajlan, L.L. Lee, and K.E. Starling, Generalized multiparameter correlation for nonpolar and polar fluid transport properties, *Ind. Eng. Chem. Res.*, *27*, p. 671, 1988.

Cramer, S.D., The solubility of methane, carbon dioxide, and oxygen in brines from 0ºC to 300ºC, *U.S. Bureau of Mines: Report No. 8706*, 16 pp., 1982.

Farrar, C.D., M.L. Sorey, W.C. Evans, J.F. Howle, B.D. Kerr, B.M. Kennedy, C.-Y. King and J.R. Southon., Forest-killing diffuse CO_2 emissions at Mammoth Mountain as a sign of magmatic unrest, *Nature*, *376* (6542), p. 675-678., 1995.

Farrar, C.D., J.M. Neil and J.F. Howle., Magmatic carbon dioxide emissions at Mammoth Mountain, California, *U.S. Geological Survey Open-File Report* 98-4217, 34p. and 1 plate, 1999.

Hepple, R. and S.M. Benson, Implications of surface seepage on the effectiveness of geologic storage of carbon dioxide as a climate change mitigation strategy, in Proceedings of the Sixth International Conf. on Greenhouse Gas Technologies GHGT-6, Kyoto, Japan., October 1–4, 2002.

Holloway, S., Safety of the underground disposal of carbon dioxide, *Energy Convers.*

Mgmt., *38 Supplement*, S241–S245, 1997.

IEA (International Energy Agency), Carbon Dioxide Utilization, *IEA Greenhouse Gas R&D Programme*, 1997; Table 6.

Kabwe, L.K., M.J. Hendry, G.W. Wilson, and J.R. Lawrence, Quantifying CO_2 fluxes from soil surfaces to the atmosphere, *J. Hydrology*, *260*(1), 1–14, 2002.

Lindeberg, E., Escape of CO2 from aquifers, *Energy Convers. Mgmt.*, *38 Supplement*, S235–S240, 1997.

NIOSH (National Institute of Occupational Safety and Health), Criteria for a Recommended Standard…Occupational Exposure to Carbon Dioxide, NIOSH Publication No. 76-194, U.S. GPO, Washington DC, 1976.

NIST (National Institute of Science and Technology), *NIST Database 14 Mixture Property Database, version 9.08*, U.S. Department of Commerce (Oct. 1992).

Oldenburg, C.M., S.W. Webb, K. Pruess, and G.J. Moridis, Mixing of stably stratified gases in subsurface reservoirs: a comparison of diffusion models, *Transport in Porous Media*, submitted.

Poling, B.E., J.M. Prausnitz, and J.P. O'Connell, *The properties of gases and liquids, fifth edition*, McGraw Hill, New York, 2001.

Pruess, K., C. Oldenburg, and G. Moridis, TOUGH2 User's Guide Version 2.0, Lawrence Berkeley National Laboratory Report *LBNL-43134*, 197 pp., November 1999.

Reichle, D. et al., Carbon sequestration research and development, U.S. Department of Energy, *DOE/SC/FE-1*, 1999.

Sorey, M., B. Evans, M. Kennedy, J. Rogie and A. Cook, Magmatic gas emissions from

Mammoth Mountain, *California Geology*, *52*(5), 4–16, 1999.

van Genuchten, M.Th., A closed form equation for predicting the hydraulic conductivity of unsaturated soils, *Soil Sci. Soc.*, *44*, 892, 1980.

Vargaftik, N.B., *Tables on Thermophysical Properties of Liquids and Gases*, *Second Edition*, Hemisphere Publishing Corp., London, 1975.

Webb, S.W., Gas-phase diffusion in porous media – Evaluation of an advective-dispersive formulation and the dusty-gas model for binary mixtures, *J. of Porous Media*, *1*(2), 187–199.

Table 1: Hydrogeological properties of the unsaturated zone for the base case.

Property	Value	Units
Permeability ($k_r = k_Z$)	1×10^{-12} (1 Darcy)	m^2
Porosity (ϕ)	0.2	-
Infiltration rate (i)	10.	cm yr^{-1}
Residual water saturation (S_{lr})	0.1	-
Residual gas saturation (S_{gr})	0.01	-
van Genuchten (1980) α	1×10^{-4}	Pa^{-1}
van Genuchten (1980) m	0.2	-

Table 2: CO_2 flow rates, attenuation efficiencies, and inventories after 1000 years of leakage for various leakage rates.

	Leakage Rate Scenarios		
	4×10^4 kg yr^{-1}	4×10^5 kg yr^{-1}	4×10^6 kg yr^{-1}
CO_2 injection rate (leakage)	1.27×10^{-3} kg s^{-1}	1.27×10^{-2} kg s^{-1}	1.27×10^{-1} kg s^{-1}
CO_2 seepage rate (seepage)	4.47×10^{-5} kg s^{-1}	4.31×10^{-3} kg s^{-1}	1.03×10^{-1} kg s^{-1}
Attenuation efficiency	96%	66%	19%
CO_2 gain from infiltration	1.50×10^{-5} kg s^{-1}	1.50×10^{-5} kg s^{-1}	1.50×10^{-5} kg s^{-1}
CO_2 bottom boundary loss	2.66×10^{-4} kg s^{-1}	4.52×10^{-4} kg s^{-1}	7.04×10^{-4} kg s^{-1}
CO_2 storage rate	9.73×10^{-4} kg s^{-1}	7.93×10^{-3} kg s^{-1}	2.32×10^{-2} kg s^{-1}
Seepage:Storage ratio	0.046	0.54	4.4
CO_2 Inventories (gas phase and dissolved)			
t = 0 (initial conditions)	Water: 24700. kg Gas: 7980. kg Total: 32680. kg	Water: 24700. kg Gas: 7980. kg Total: 32680. kg	Water: 24700. kg Gas: 7980. kg Total: 32680. kg
t = 1000 yrs (steady state)	Water: 315000. kg Gas: 86600. kg Total: 401600. kg	Water: 651000. kg Gas: 200000. kg Total: 851000. kg	Water: 1040000. kg Gas: 329000. kg Total: 1369000. kg

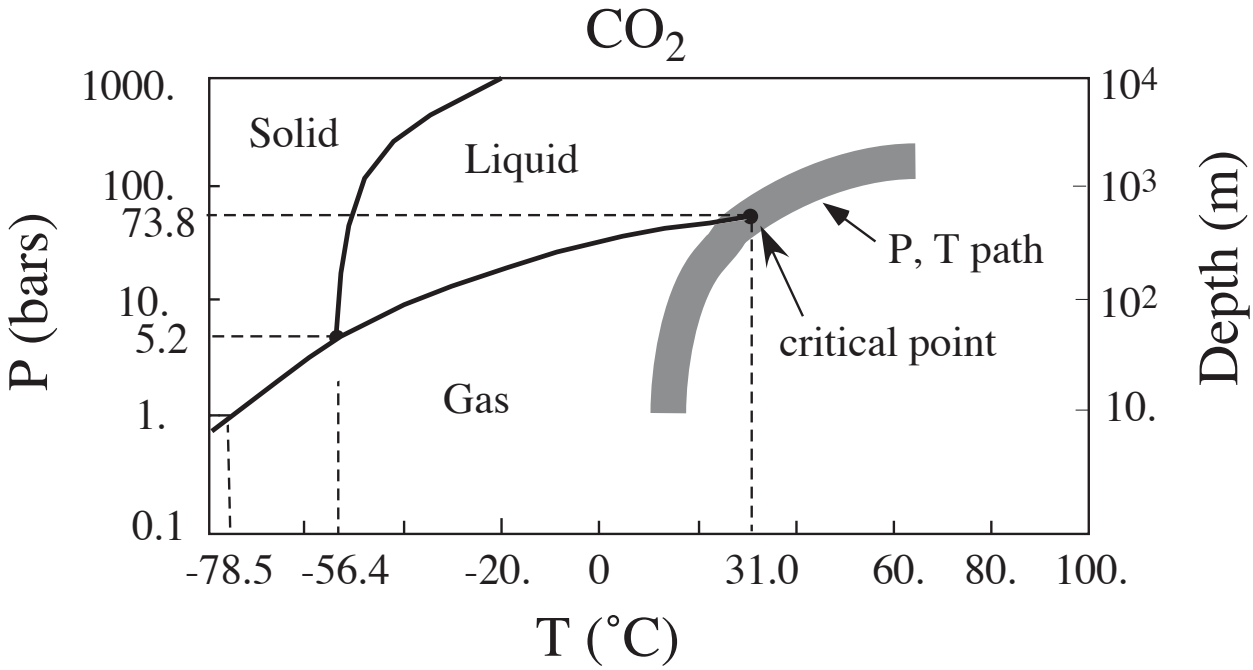

Figure 1. Phase diagram for CO_2 with approximate P, T path in the subsurface assuming hydrostatic pressure and geothermal gradient of 25 ˚C km^{-1}.

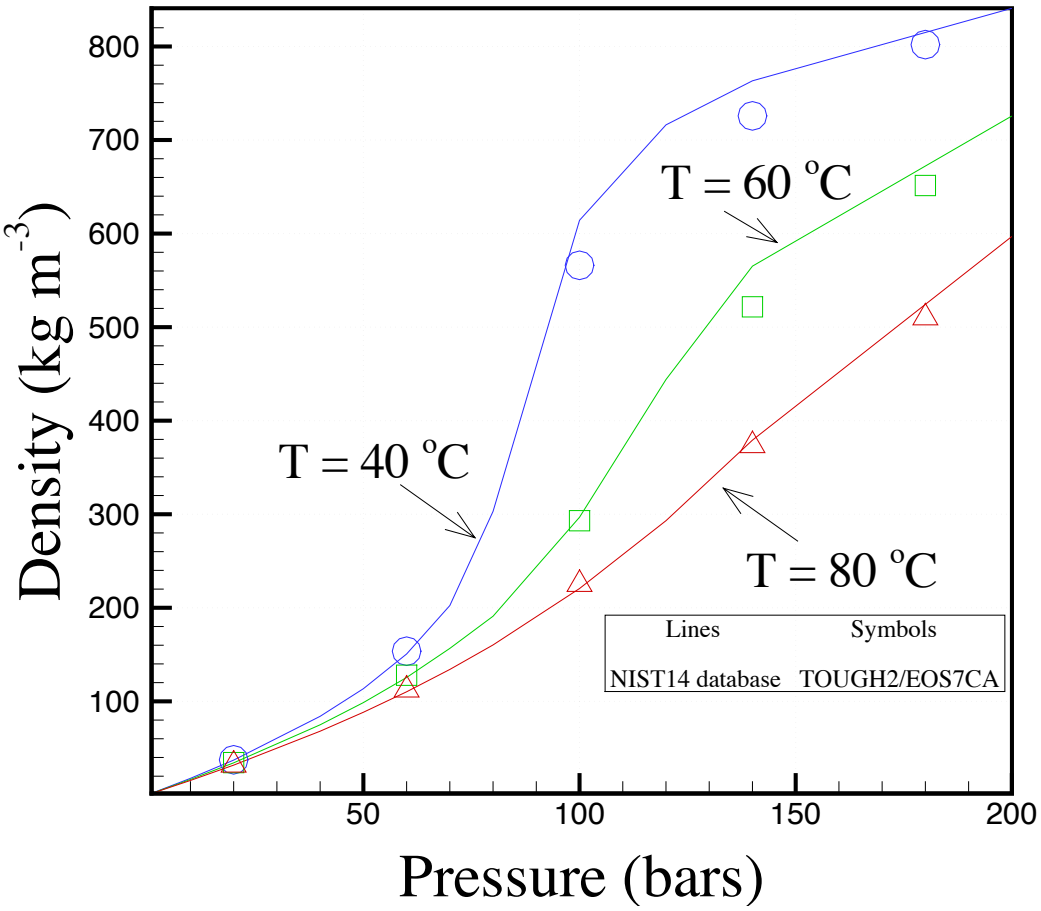

Figure 2. Density of CO_2 as a function of pressure at three different temperatures.

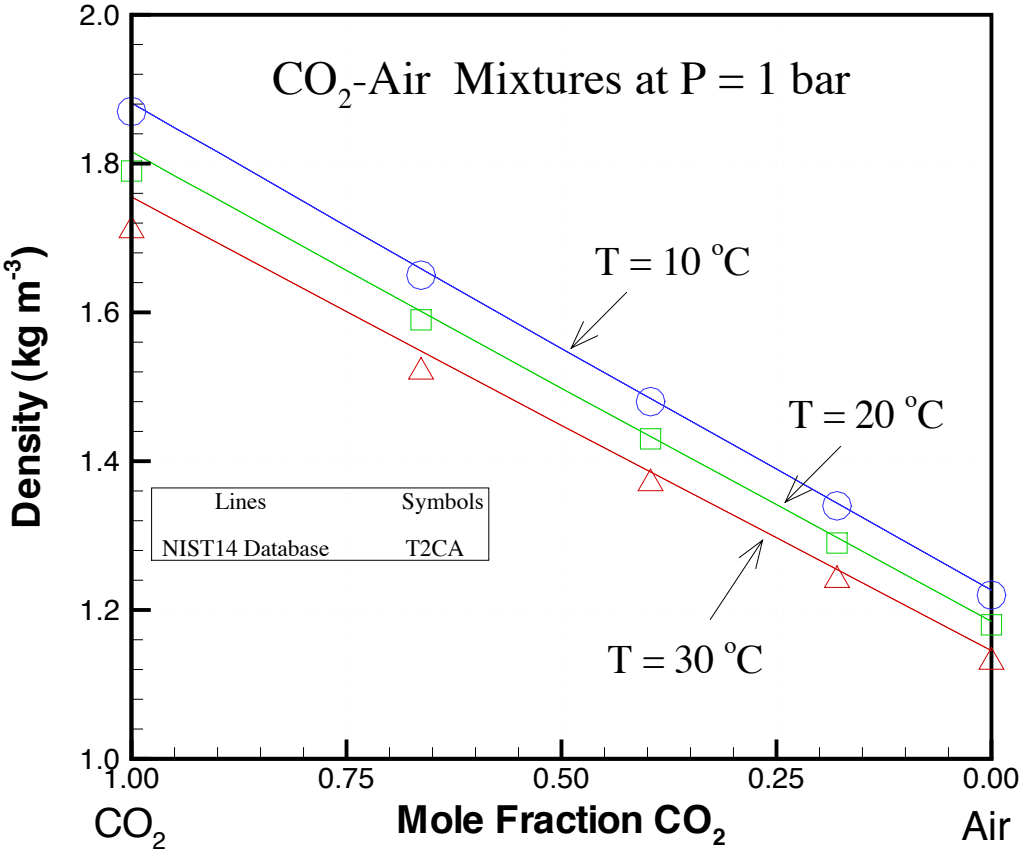

Figure 3. Density as a function of concentration in the system CO_2-air at P = 1 bar.

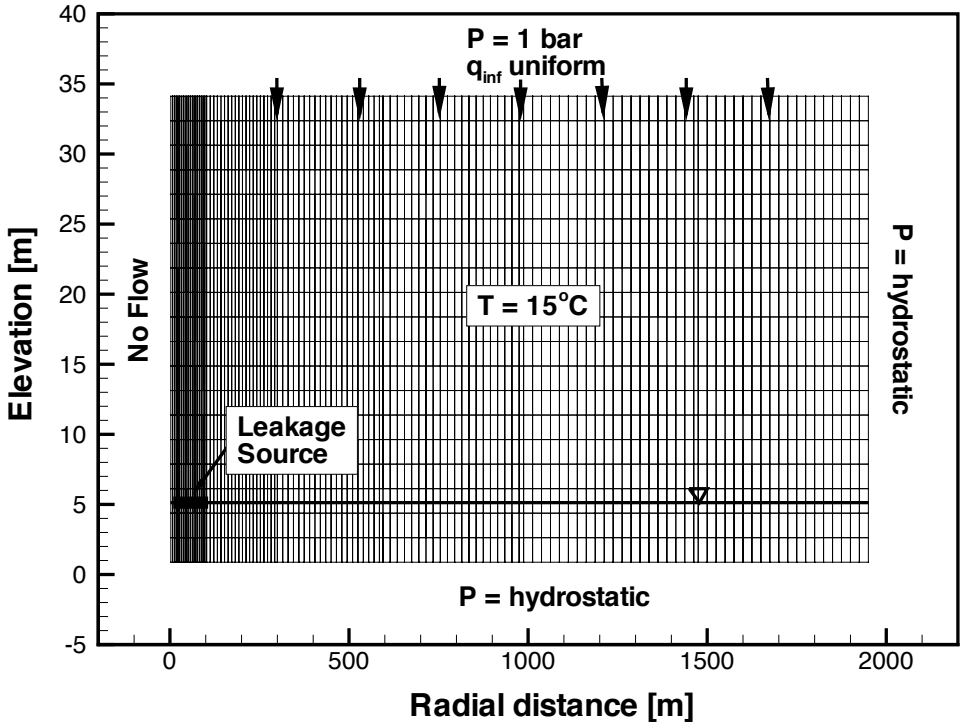

Figure 4. Conceptual model and grid for the unsaturated zone model.

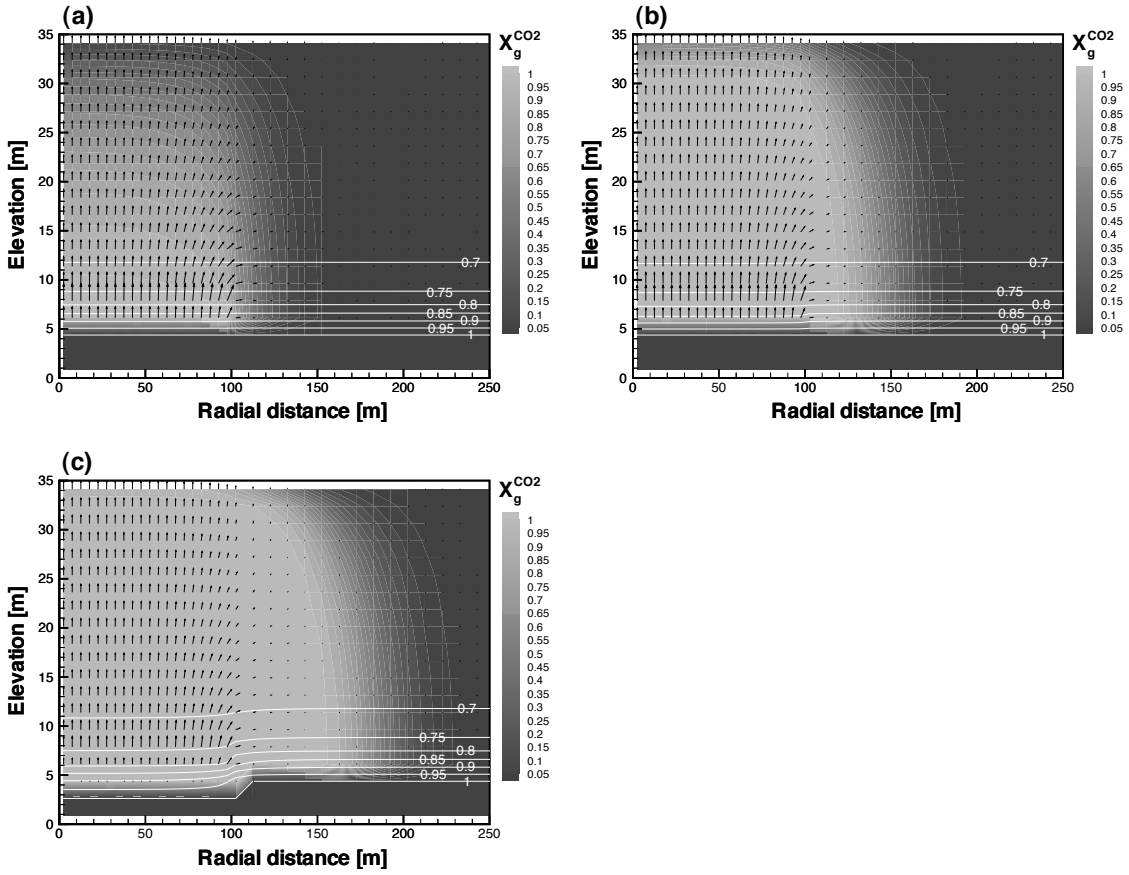

Figure 5. Shading indicates the mass fraction of CO_2 in the gas phase, labeled contour lines indicate the water saturation, and vectors indicate the pore velocity of the gas phase for the base case at steady-state seepage rates with a leakage rate of (a) 4×10^4 kg yr^{-1}, (b) 4×10^5 kg yr^{-1} and (c) 4×10^6 kg yr^{-1}. The maximum vector size represents a value of approximately (a) 0.057 m d^{-1}, (b) 0.53 m d^{-1} and (c) 3.6 m d^{-1}

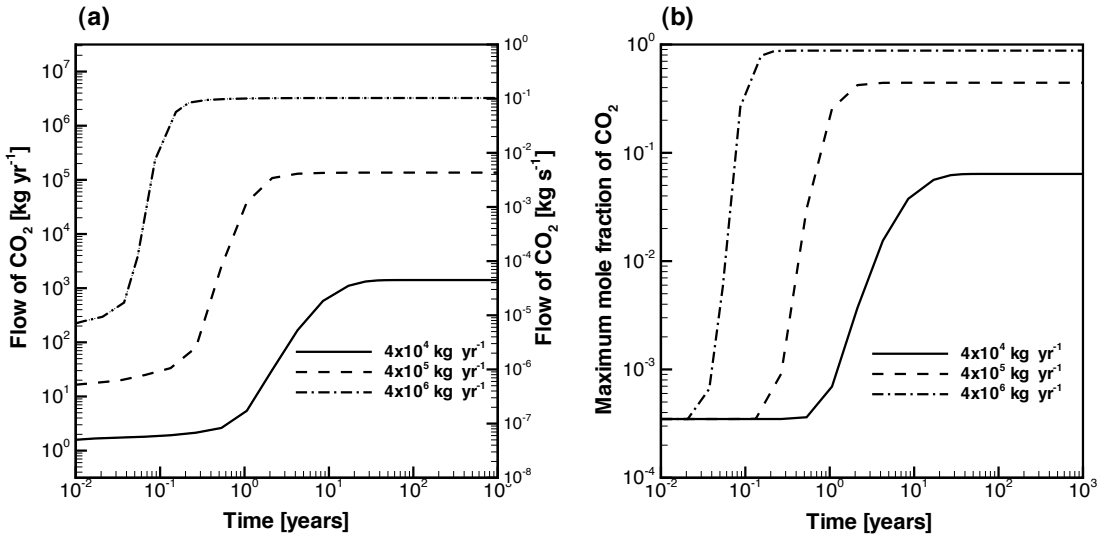

Figure 6. Total flow rate of CO_2 across the top boundary and maximum mole fraction of CO_2 in the gas phase at the top of the system as a function of time after leakage enters the unsaturated zone.

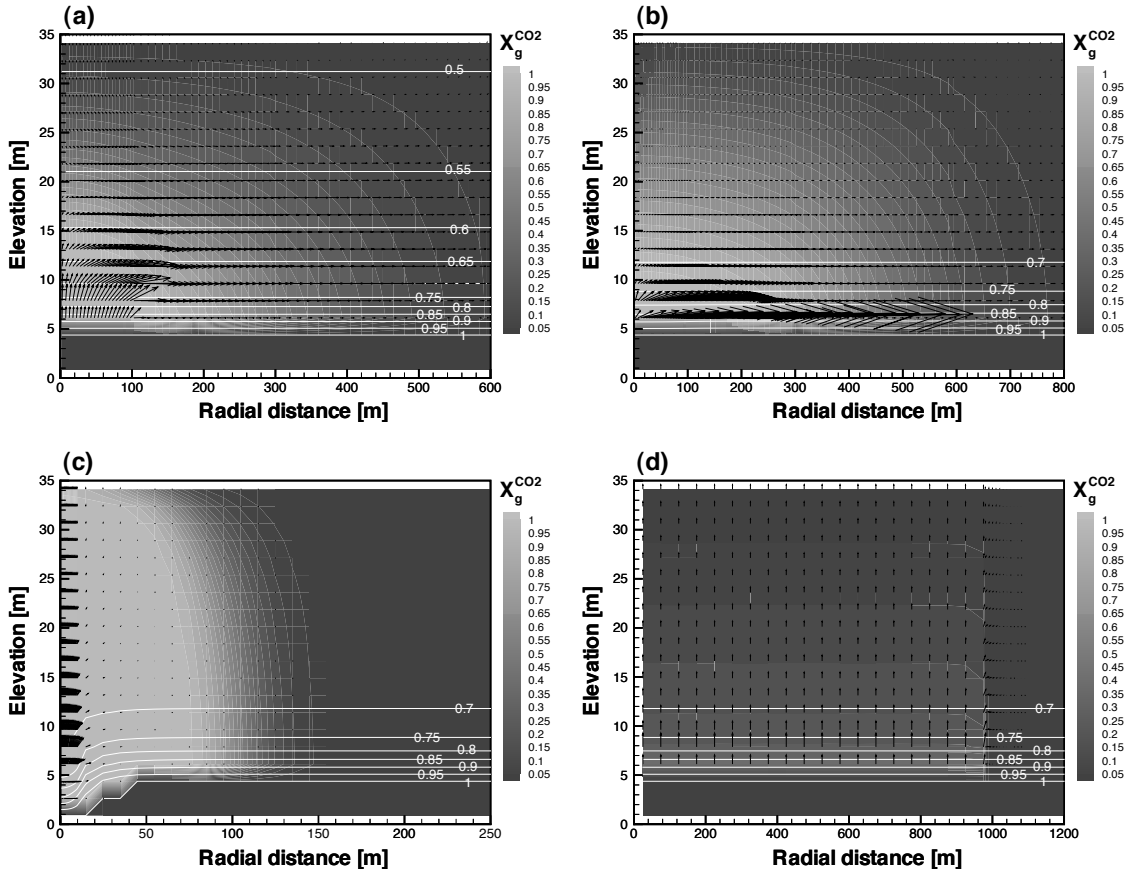

Figure 7. Shading indicates the mass fraction of CO_2 in the gas phase, labeled contour lines indicate the water saturation, and vectors indicate the pore velocity of the gas phase for a leakage rate of 4×10^5 kg yr^{-1} and at steady state seepage rates with (a) a permeability of 1×10^{-9} m^2, (b) an anisotropy of 1000:1, (c) a source radius of 10 m and (d) a source radius of 1000 m. The maximum vector size represents a value of approximately (a) 1.0 m d^{-1}, (b) 8.4 m d^{-1} (c) 17 m d^{-1} and (d) 0.0048 m d^{-1}.

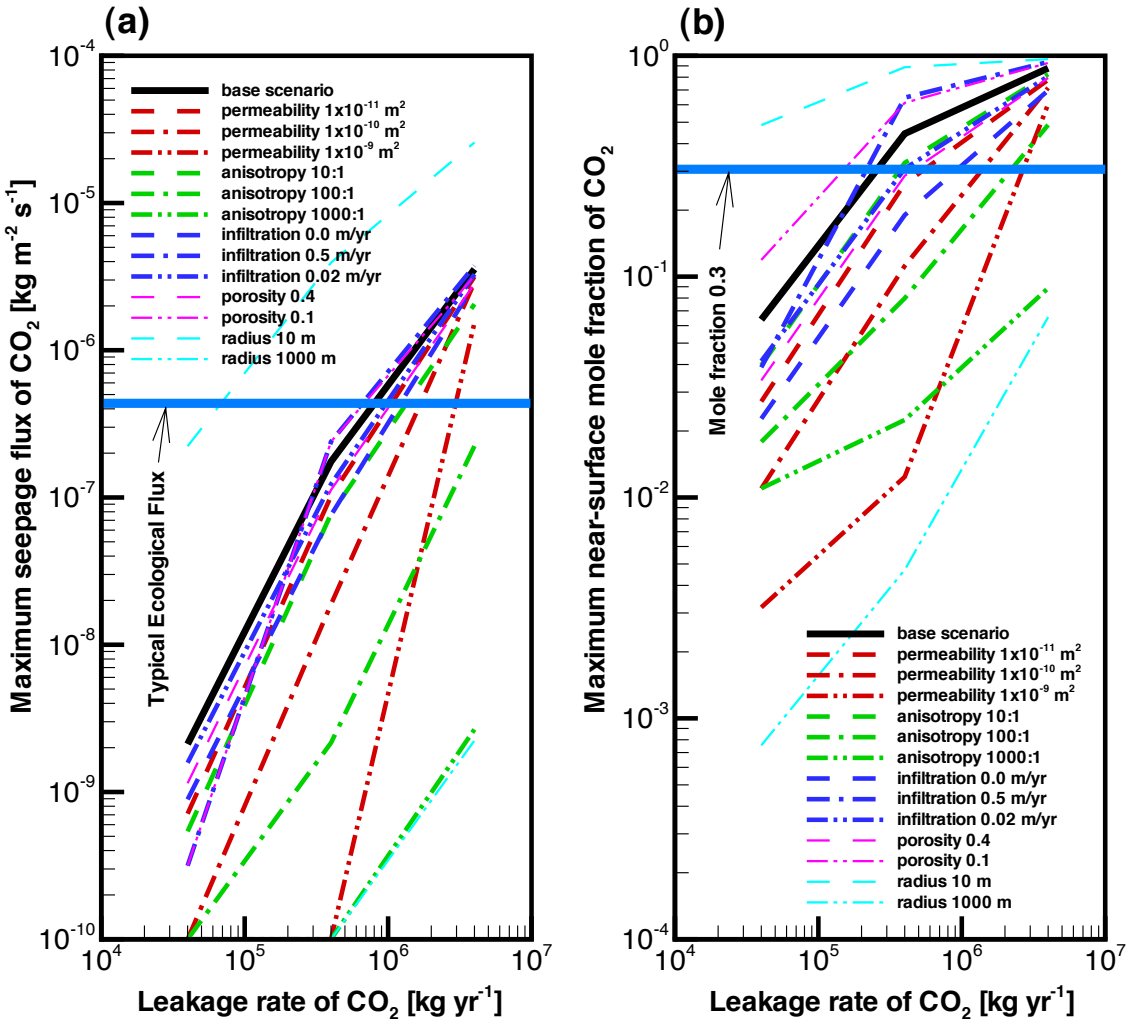

Figure 8. The maximum seepage flux of CO_2 and the maximum near-surface mole fraction of CO_2 as a function of leakage rate at steady-state seepage conditions.

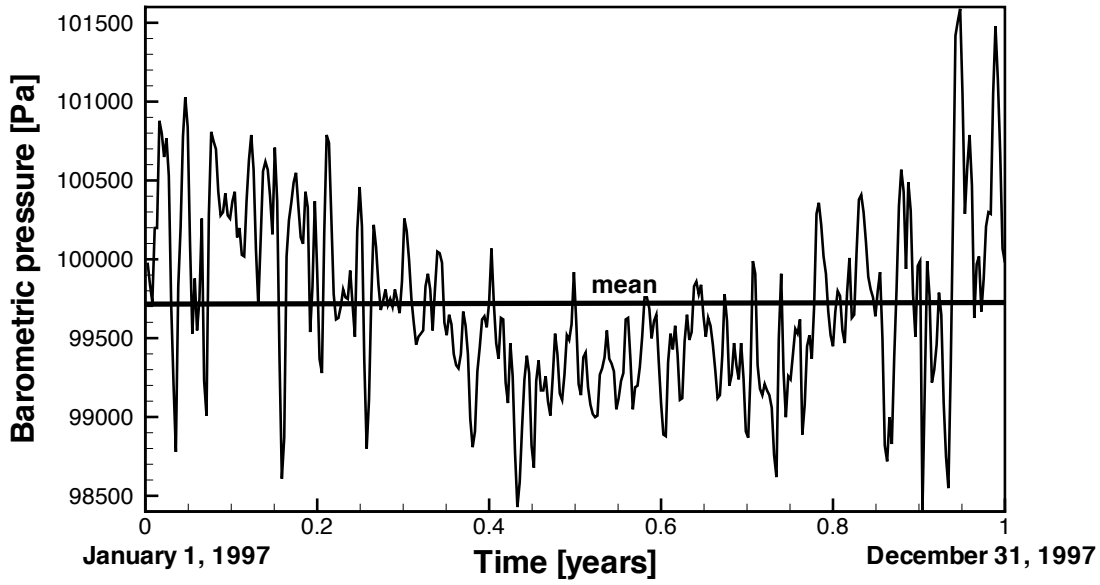

Figure 9. Barometric pressure used as top boundary condition.

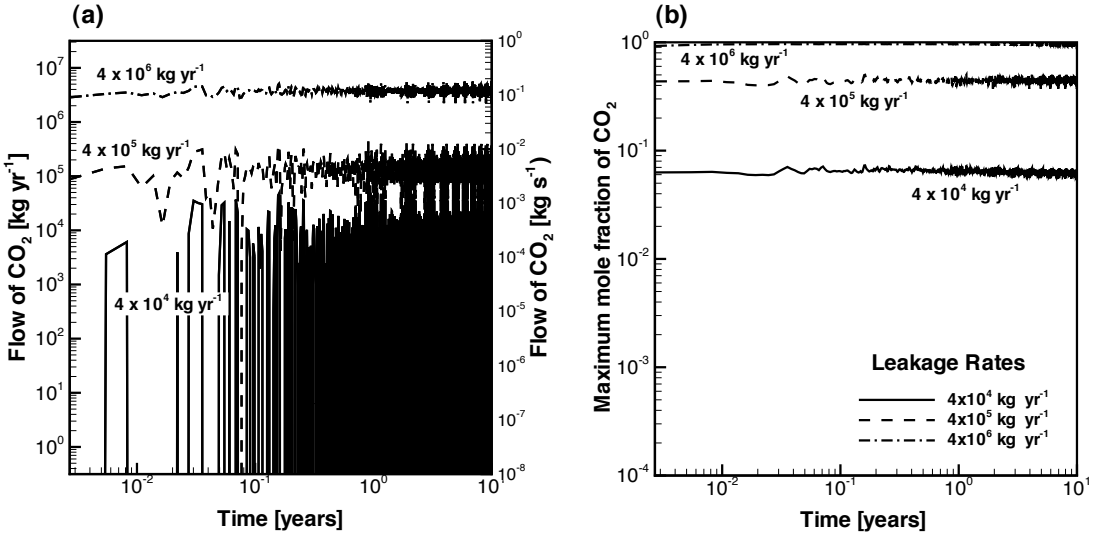

Figure 10. Temporal evolution of (a) total surface flow of CO_2 and (b) maximum near-surface mole fraction of CO_2 for the base case with variable-pressure top boundary condition.

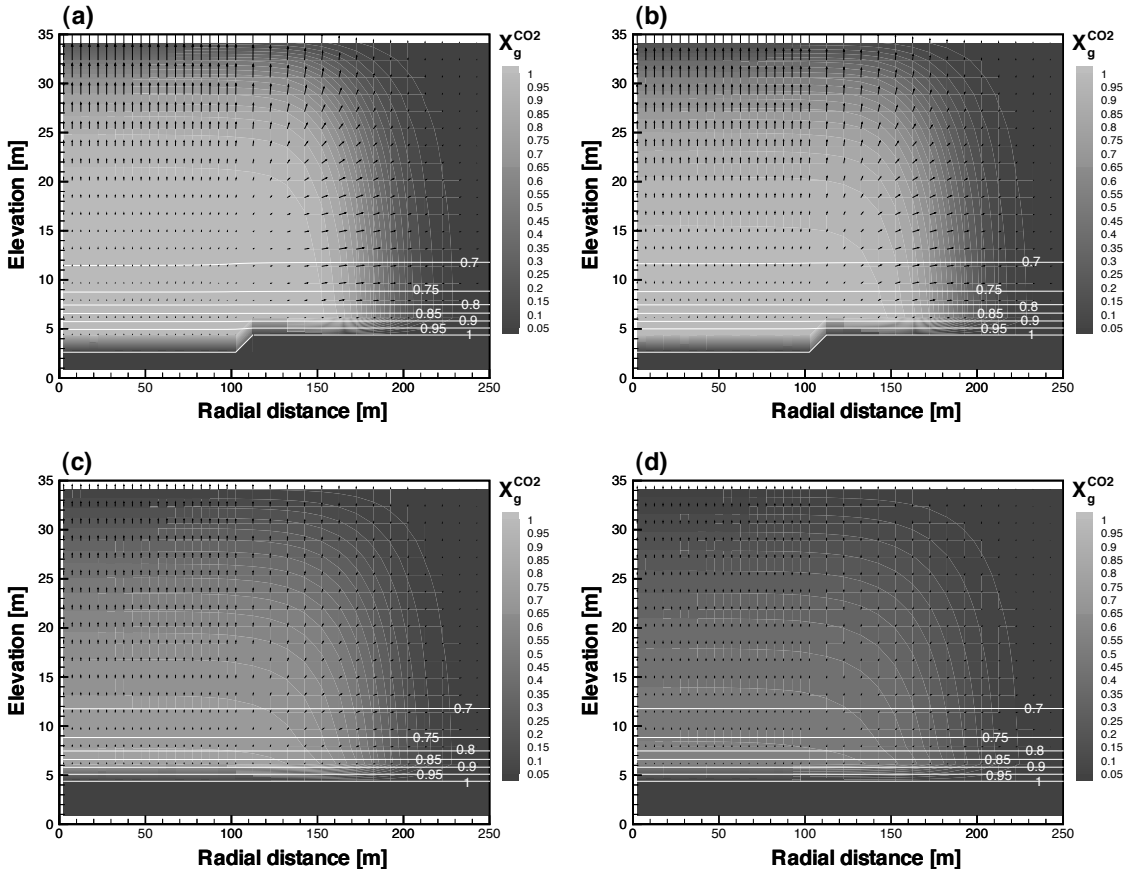

Figure 11. Shading indicates the mass fraction of CO_2 in the gas phase and labeled contour lines indicate the water saturation for the case of zero leakage and an initial CO_2 plume present in the unsaturated zone. (a) t = 6 months, (b) t = 1 year, (c) t = 5 years, and (d) t = 10 years. The maximum vector size represents a value of approximately (a) 2.8 x 10^{-2} m d^{-1}, (b) 2.0 x 10^{-2} m d^{-1}, (c) 7.5 x 10^{-3} m d^{-1}, and (d) 3.9 x 10^{-3} m d^{-1}.